



HAL
open science

Monte Carlo power iteration: Entropy and spatial correlations

Michel Nowak, Jilang Miao, Eric Dumonteil, Benoit C. Forget, Anthony Onillon, Kord S Smith, Andrea Zoia

► **To cite this version:**

Michel Nowak, Jilang Miao, Eric Dumonteil, Benoit C. Forget, Anthony Onillon, et al.. Monte Carlo power iteration: Entropy and spatial correlations. *Annals of Nuclear Energy*, 2016, 94, pp.856-868. 10.1016/j.anucene.2016.05.002 . cea-02486077

HAL Id: cea-02486077

<https://cea.hal.science/cea-02486077>

Submitted on 20 Feb 2020

HAL is a multi-disciplinary open access archive for the deposit and dissemination of scientific research documents, whether they are published or not. The documents may come from teaching and research institutions in France or abroad, or from public or private research centers.

L'archive ouverte pluridisciplinaire **HAL**, est destinée au dépôt et à la diffusion de documents scientifiques de niveau recherche, publiés ou non, émanant des établissements d'enseignement et de recherche français ou étrangers, des laboratoires publics ou privés.

Monte Carlo power iteration: entropy and spatial correlations

Michel Nowak^a, Jilang Miao^b, Eric Dumonteil^{a,c}, Benoit Forget^b, Anthony Onillon^c, Kord S. Smith^b, Andrea Zoia^{a,*}

^aDen-Service d'études des réacteurs et de mathématiques appliquées (SERMA), CEA, Université Paris-Saclay, F-91191, Gif-sur-Yvette, France

^bDepartment of Nuclear Science and Engineering, Massachusetts Institute of Technology, 77 Massachusetts Avenue, 24-107, Cambridge, MA 02139, United States

^cIRSN, 31 Avenue de la Division Leclerc, 92260 Fontenay aux Roses, France

Abstract

The behaviour of Monte Carlo criticality simulations is often assessed by examining the convergence of the so-called entropy function. In this work, we shall show that the entropy function may lead to a misleading interpretation, and that potential issues occur when spatial correlations induced by fission events are important. Additional information can be extracted from the analysis of the higher-order moments of the entropy function, or from the center of mass of the neutron population. Within the framework of a simplified model based on branching processes, we will relate the behaviour of the spatial fluctuations of the fission chains to the key parameters of the simulated system, namely, the number of particles per generation, the reactor size and the migration area. Numerical simulations of a fuel rod and of a whole core suggest that the obtained results are quite general and hold true also for real-world applications.

Keywords: Entropy, Clustering, Power iteration, OpenMC, TRIPOLI-4[®]

1. Introduction

Monte-Carlo simulation is often used in criticality calculations to assess the asymptotic distribution of the neutron population within a system, which corresponds to the fundamental eigenmode of the Boltzmann critical equation (Lux and Koblinger, 1991). The most widely used and simplest numerical method allowing the neutron population to converge to the fundamental eigenmode is the power iteration (Lux and Koblinger, 1991; Rief and Kschwendt, 1967; Brown, 2005): in Monte Carlo methods, an initial arbitrary source particle distribution is transported until all neutrons have been either absorbed or leaked (forming a so-called generation). The secondary neutrons coming from the fission events within a generation g are banked and provide the source for the following generation $g + 1$. The algorithm is then iterated over many generations, until the fission sources for a sufficiently large g statistically attain a spatial and energetic equilibrium, as ensured by the power iteration method. The effects of higher eigenmodes on the neutron population are expected to fade away, and eventually the neutron population will be distributed according to the fundamental eigenmode. The ratio between the population size at generation $g + 1$ and the population size at generation g converges to the fundamental eigenvalue k_{eff} for large g (Lux and Koblinger, 1991).

In this context, two key issues are known to affect the neutron population during power iteration and have therefore attracted intensive research efforts: fission source convergence and correlations.

Concerning the former, a slow exploration of the viable phase space by the population implies a poor source convergence. In particular, it has been shown that the convergence of k_{eff} might be faster than that of the associated fundamental eigenmode, which is expected on physical grounds, the former being an integral property of the system and the latter being a local property (Lux and Koblinger, 1991). The rate of convergence depends on the separation between the first and the second eigenvalue of the Boltzmann equation, the so-called dominance ratio: the closer to one the dominance ratio becomes, the poorer the convergence (Lux and Koblinger, 1991; Ueki et al., 2004; Dumonteil and Malvagi, 2012). If Monte-Carlo tallies are scored before attaining equilibrium, biases on the estimation of the variance may appear, and monitoring the convergence of k_{eff} might be insufficient so as to determine the convergence of the whole population (Ueki and Brown, 2003; Dumonteil et al., 2006; LAbbate et al., 2007; Ueki, 2005).

Several tools have been proposed to assess the spatial convergence of fission sources, among which, one of the most popular, is the entropy of the fission sources (Ueki et al., 2003; Ueki, 2012; Ueki and Brown, 2003; Ueki, 2005). The idea behind the entropy function is to superimpose a regular Cartesian mesh to the viable space and to record the number of fission sites for each cell of the mesh, at each generation. This allows computing the so-called Shannon entropy \mathcal{S} (Li and Vitany, 1997), which is defined as

$$\mathcal{S}(g) = - \sum_{i,j,k} p_{i,j,k}(g) \log_2[p_{i,j,k}(g)], \quad (1)$$

where $p_{i,j,k}(g)$ is the (statistically weighted) number of fission source particles in the cell of index i, j, k at generation g divided by the total number of source particles in all cells at generation

*Corresponding author. Tel. +33 (0)1 6908 9544
Email addresses: jlmiao@mit.edu (Jilang Miao),
andrea.zoia@cea.fr (Andrea Zoia)

g. The entropy function is expected to provide a measure of the phase space exploration as a function of the number of generations (Li and Vitany, 1997; Cover and Thomas, 1991): when the neutron distribution attains its stationary shape, the entropy \mathcal{S} converges. A prominent advantage of the entropy is that \mathcal{S} is a single scalar value whose evolution condenses the required information on the spatial repartition. Moreover, as apparent from Eq. (1), the entropy \mathcal{S} of the source distribution at generation g is bounded, namely,

$$0 \leq \mathcal{S}(g) \leq \log_2 B, \quad (2)$$

where B is the number of cells of the spatial mesh. This property ensures in particular that the variations of \mathcal{S} will be bounded, and that the highest value of the entropy will be reached in the case of a perfect equipartition. The entropy function is nowadays a standard tool for most production Monte Carlo codes, although some concerns have been raised about possible issues related to its use in convergence diagnostics for loosely coupled multiplying systems (see, e.g., the analysis in (Shi and Petrovic, 2010a,b; Ueki, 2005)).

The latter issue with power iteration in Monte Carlo simulation concerns the impact of correlations induced by fission events: physically speaking, a neutron can only be generated in the presence of a parent particle, which induces generation-to-generation correlations (Lux and Koblinger, 1991; Sjenitzer and Hoogenboom, 2011). This is a widely recognized problem, which is expected to affect the convergence of Monte Carlo scores and in particular make the applicability of Central Limit Theorem questionable (Ueki, 2012; Brown, 2009; Ueki, 2005). Correlations between generations have been often studied within the mathematical framework provided by the eigenvalue analysis of the Boltzmann critical equation (Brown, 2005; Sutton, 2014). Further work on correlations has concerned techniques aimed at improving the standard deviation estimates of Monte Carlo scores (Gelbard and Prael, 1990; Ueki et al., 2003, 2004; Dumonteil and Malvagi, 2012; Ueki, 2005). More recently, it has been pointed out that, due to the asymmetry between correlated births by fission and uncorrelated deaths by capture and leakage¹, neutrons initially prepared at equilibrium will be preferentially found clustered close to each other after a few generations (Dumonteil et al., 2014). This peculiar phenomenon, named neutron clustering, might induce a strongly heterogeneous spatial repartition of the neutron population, which randomly evolves between generations (Dumonteil et al., 2014; Zoia et al., 2014; de Mulatier et al., 2015). The impact of neutron clustering has been determined to be inversely proportional to the number of neutrons per generation (Dumonteil et al., 2014).

In this paper, we will show that neutron clustering, not surprisingly, also affects the convergence of the fission sources: because of fission-induced correlations, the entropy function

might in turn be ineffective at detecting potential deviations of the neutron population with respect to the expected equilibrium.

This manuscript is organized as follows. In Sec. 2, we will initially consider a simplified reactor model where exact analytical results can be established, and show that in some cases the convergence of the entropy is achieved, although the neutron population is still affected by strong spatial fluctuations. Then, in Sec. 3, we will refine our analysis based on the spatial moments of the entropy function and on the center of mass of the neutron population: these statistical tools can be used together with regular entropy so as to extract information concerning the simulated system, and thus improve the diagnosis of fission source equilibrium. In Sec. 4 we will then relate the behaviour of such spatial fluctuations to the key system parameters, namely, the reactor size, the number of neutrons per generation, and the migration area, based on the theory of branching processes. In Sec. 5 we will numerically explore the behaviour of a fuel rod and a full core with detailed geometry and compositions and continuous-energy treatment, and show that the theoretical findings for the simple reactor model actually apply more generally to realistic configurations. Conclusions will be drawn in Sec. 6.

2. Neutrons in a box and the behaviour of the entropy

In order to assess the behaviour of the entropy function in the presence of fission-induced correlations, we will work out an example that is simple enough for exact results to be analytically derived and compared to the Monte Carlo simulations, and yet retains the key physical features of a real system (Miao et al., 2016).

Let us therefore consider a prototype model of a reactor core consisting of a collection of N neutrons undergoing scattering, capture and fission within a box of volume $V = L^3$. To simplify the matter, we will assume that neutrons can only be reflected at the boundaries. The random displacements of the neutrons will be modelled by branching exponential flights with constant speed v ; scattering and fission will be taken to be isotropic in the center of mass frame. The physical parameters of this prototype reactor will be the following:

$$\Sigma_s = 0.27, \quad \Sigma_c = 0.02, \quad \Sigma_f = \frac{\Sigma_c}{\bar{\nu} - 1.0}, \quad (3)$$

where Σ_s is the scattering cross section, Σ_c is the capture cross section, and Σ_f is the fission cross section (in cm^{-1}). The parameter $\bar{\nu}$ denotes the average number of secondary neutrons per fission. Observe that on the basis of the cross sections defined above the system is exactly critical, i.e.,

$$k_{eff} = \frac{\bar{\nu}\Sigma_f}{\Sigma_c + \Sigma_f} = 1, \quad (4)$$

for any choice of $\bar{\nu}$. For our simulations, we have set $\bar{\nu} = 2.5$. The fundamental eigenmode associated to $k_{eff} = 1$ corresponds to an equilibrium distribution that is spatially homogeneous over the box, as expected on physical grounds.

¹This phenomenon has been first investigated in the context of theoretical ecology, especially in relation to the evolution of biological communities: see, e.g., (Young et al., 2001; Houchmandzadeh, 2008), and can be better understood in the framework of branching random walks (Athreya and Ney, 1972; Williams, 1974; Pázsit and Pál, 2008; Zoia et al., 2012).

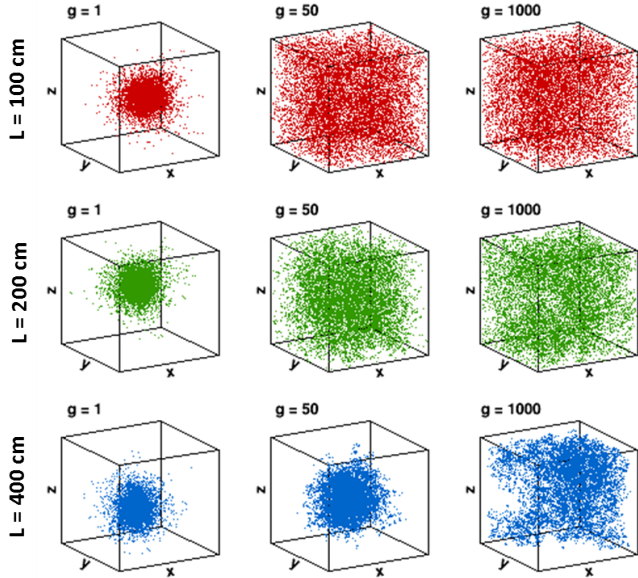


Figure 1: Distribution of fission sites during Monte Carlo power iteration as a function of generations g , for three different reactor sizes L . The guess source at $g = 0$ consists of $N = 10^4$ neutrons located at the center of the cube. Power iteration is run for 1000 generations. Top: $L = 100$ cm; center: $L = 200$ cm; bottom: $L = 400$ cm.

This prototype reactor model can be easily implemented and solved by power iteration within a Monte Carlo code. In order to probe the effects of neutron clustering on the convergence of power iteration, we have performed several Monte Carlo critical simulations of such system by varying the number N of particles per generation and the size L of the box, the other physical parameters being unchanged. For all configurations, we have assumed that the power iteration is started with a point source consisting of N neutrons located at the center of the box. As the number of generation increases, the neutron population spreads over the whole box, and is forced to converge towards the fundamental eigenmode by the power iteration. However, this spread is counter-reacted by the spatial correlations induced by fission chains, and clustering might then come into play.

The distribution of the fission sites as obtained during the power iteration for a fixed number $N = 10^4$ of initial particles and different box sizes L is displayed in Fig. 1. When the neutron density is high (i.e., L is small for a given N), the fission sites converge to an equilibrium configuration where neutrons are homogeneously spread over the whole volume, with mild fluctuations mostly due to scattering. As L increases, spatial fluctuations due to the competing mechanisms of fission, absorption and scattering become more apparent. For even larger L , the neutron population displays patchiness, with neutrons randomly moving around the box grouped into a large cluster. Previous investigations based on the diffusion theory approximation have indeed shown that spatial clustering is quenched when $L^2 \ll N\mathcal{M}^2$, where \mathcal{M}^2 is the migration area (de Mulatier et al., 2015). Fluctuations due to correlations are therefore ex-

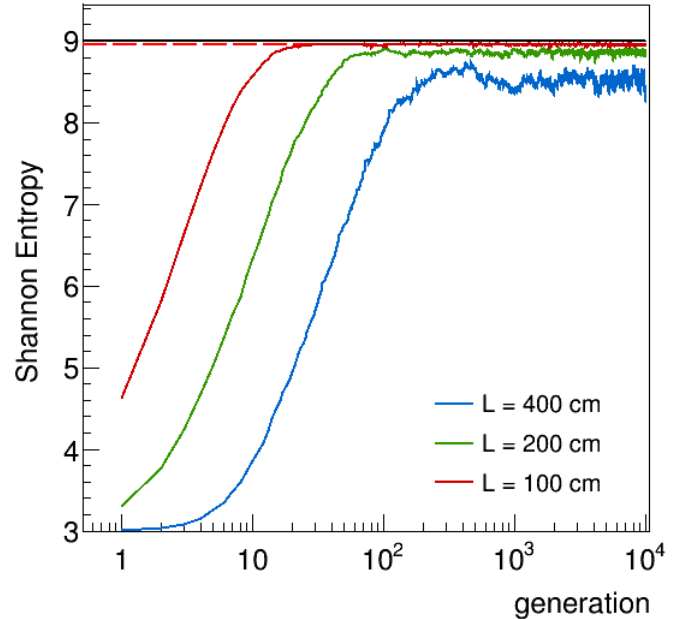


Figure 2: Homogeneous cube reactor. The behaviour of the measured Shannon entropy $\mathcal{S}(g)$ during Monte Carlo power iteration as a function of generations g , for three different reactor sizes L and fixed number N of neutrons per generation. The guess source at $g = 0$ consists of $N = 10^4$ neutrons located at the center of the cube. Power iteration is run for 1000 generations. Upper red curve: $L = 100$ cm; central green curve: $L = 200$ cm; lower blue curve: $L = 400$ cm. The dashed red line represents the expected entropy value \mathcal{S}_N as in Eq. (6), and the solid black line is the ideal expected entropy \mathcal{S}_∞ for an infinite number of particles per generation as in Eq. (5).

pected to decrease for decreasing box size L when keeping N constant, which is coherent with our numerical findings.

It is instructive to compute the Shannon entropy $\mathcal{S}(g)$ for the power iteration simulations examined here. To fix the ideas, we will assume that each box side L is partitioned into 8 spatial meshes, which implies $B = 8^3 = 512$. For the simple model considered in this Section, the theoretical ideal entropy associated to the fundamental eigenmode, i.e., the expectation of $\log(p)$ corresponding to a uniform spatial distribution, can be exactly computed, and reads

$$\mathcal{S}_\infty = \log_2(B) = 9. \quad (5)$$

Actually, for a finite number N of particles per generation, the theoretical expected Shannon entropy is always lower than the ideal value \mathcal{S}_∞ . For the homogeneous reactor, the expected Shannon entropy at finite N can be explicitly computed (derivation is provided in Appendix A) and reads

$$\mathcal{S}_N = \log_2(N) - \frac{B^{1-N}}{N} \sum_{k=0}^N \binom{N}{k} (B-1)^{N-k} k \log_2(k), \quad (6)$$

which depends on the number of spatial meshes B and of the

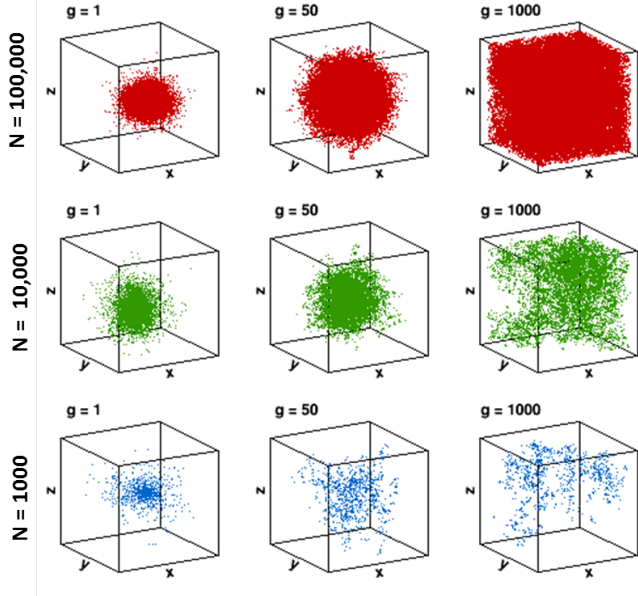


Figure 3: Homogeneous cube reactor. Distribution of fission sites during Monte Carlo power iteration as a function of generations g , for three different initial population sizes N and fixed $L = 400$ cm. The guess source at $g = 0$ consists of N neutrons located at the center of the cube. Power iteration is run for 1000 generations. Top: $N = 10^5$; center: $N = 10^4$; bottom: $N = 10^3$.

number of particles N . It can be shown that $\mathcal{S}_N < \mathcal{S}_\infty$; when the number of neutrons N is very large, the expected entropy converges to the ideal reference value, namely, $\mathcal{S}_N \rightarrow \mathcal{S}_\infty$. In the following, we will compare the measured entropy $\mathcal{S}(g)$ as a function of generations to the expected value \mathcal{S}_N .

The behaviour of the measured entropy $\mathcal{S}(g)$ corresponding to the reactor configurations presented in Fig. 1 is displayed in Fig. 2. The number m of generations taken by the neutron population to achieve spatial convergence (i.e., to explore the whole reactor) starting from a point source can be roughly estimated by $m \simeq L^2/\ell^2$, ℓ^2 being the mean square displacement of a particle per generation. The quantity ℓ^2 can be estimated during the Monte Carlo simulation, and for the example discussed here we have $\ell^2 \simeq 175$ cm² for $L = 100$ cm, $\ell^2 \simeq 185$ cm² for $L = 200$ cm, and $\ell^2 \simeq 190$ cm² for $L = 400$ cm, which yields $m \simeq 57$ for $L = 100$ cm, $m \simeq 215$ for $L = 200$ cm, and $m \simeq 830$ for $L = 400$ cm, respectively. This is consistent with the number of generations taken by the measured entropy $\mathcal{S}(g)$ to attain convergence, as shown in Fig. 2.

When $L = 100$ cm, the computed $\mathcal{S}(g)$ asymptotically converges to the expected value \mathcal{S}_N for large g : in this case, the entropy function correctly mirrors the equilibrium attained by the neutron population. As L increases by keeping N fixed, spatial clustering strongly affects the neutron population during the power iteration: the neutron population still attains a stationary equilibrium distribution, which is nonetheless quite different from the flat fundamental eigenmode. In particular, a larger fraction of empty cells is observed. The measured entropy $\mathcal{S}(g)$ consequently converges to an asymptotic value for

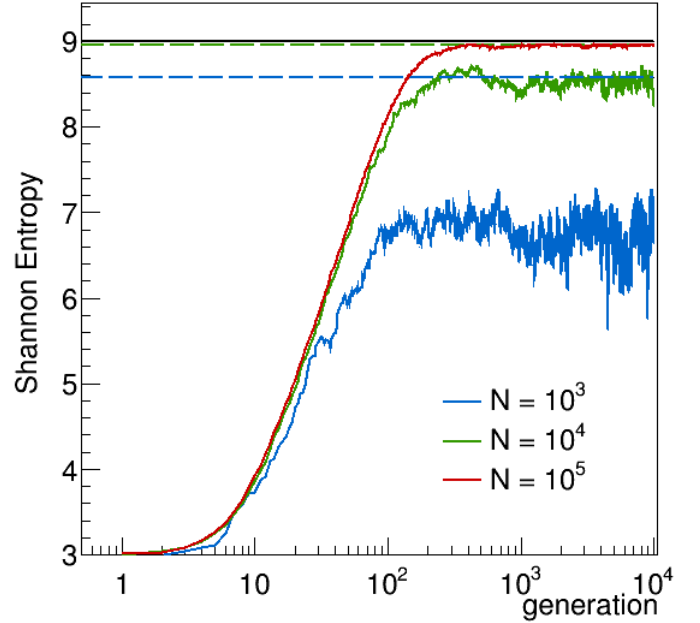


Figure 4: Homogeneous cube reactor. The behaviour of the measured Shannon entropy $\mathcal{S}(g)$ during Monte Carlo power iteration as a function of generations g , for different initial population sizes N and fixed $L = 400$ cm. The guess source at $g = 0$ consists of N neutrons located at the center of the cube. Power iteration is run for 1000 generations. Upper red curve: $N = 10^5$; central green curve: $N = 10^4$; lower blue curve: $N = 10^3$. The dashed lines represent the expected entropy value \mathcal{S}_N as in Eq. (6) (red: $N = 10^5$, green: $N = 10^4$ and blue: $N = 10^3$, respectively), and the solid black line is the ideal expected entropy \mathcal{S}_∞ for an infinite number of particles per generation as in Eq. (5).

large g which is lower than the expected \mathcal{S}_N and decreases with increasing L . Numerical analysis shows that the ratio between the measured and the asymptotic value of the Shannon entropy scales as $\mathcal{S}(g)/\mathcal{S}_N \propto 1/L$ for fixed N .

For the homogeneous reactor examined here, where \mathcal{S}_N can be exactly determined, measuring the discrepancy between $\mathcal{S}(g)$ and \mathcal{S}_N at convergence allows in principle the anomalous behaviour of the fission source convergence to be detected. In general, however, it is not possible to compute the expected entropy value \mathcal{S}_N , which means that in the presence of strong spatial clustering assessing the convergence of the Shannon entropy may turn out to be insufficient to ensure a proper spatial convergence of the fission sources.

We have carried a similar analysis for the power iteration by varying the number N of initial neutrons per generation at fixed reactor size L . The results are displayed in Figure 3. The pattern followed by the neutron population during convergence is similar to that discussed in the analysis carried out above. When the neutron density is high (i.e., N is large for a given L), the fission sites converge to a spatial equilibrium with neutrons

200 homogeneously distributed over the whole volume, with mild
 fluctuations mostly due to scattering. As N decreases, spatial
 fluctuations become more apparent, and for even smaller pop-
 ulations neutron clustering eventually sets in. On the basis of
 the argument discussed above, fluctuations due to correlations
 205 are expected to increase for decreasing population size N when
 keeping L constant, which is coherent with our numerical find-
 ings.

The behaviour of the measured Shannon entropy $\mathcal{S}(g)$ for the
 configurations presented in Fig. 3 is displayed in Fig. 4. The
 210 expected entropy value \mathcal{S}_N depends on the number of particles
 per generation, whereas the ideal asymptotic value \mathcal{S}_∞ is un-
 changed and reads $\mathcal{S}_\infty = 9$. The number m of generations taken
 by the neutron population to achieve spatial convergence start-
 ing from the point source is again $m \simeq L^2/\ell^2$, with $\ell^2 \simeq 190$
 215 cm^2 and $L = 400 \text{ cm}$, which yields $m \simeq 830$, independently of
 the number of simulated neutrons. This is consistent with the
 number of generations taken by the measured entropy $\mathcal{S}(g)$ to
 attain convergence, as shown in Fig. 4.

When the number of initial neutrons N is sufficiently large,
 220 the Shannon entropy converges to an asymptotic value that is
 very close to \mathcal{S}_N . As the relevance of the spatial cluster-
 ing increases for decreasing N , the fraction of empty cells at equi-
 librium increases, and the asymptotic value of $\mathcal{S}(g)$ attained at
 convergence becomes progressively lower than \mathcal{S}_N . Numerical
 225 analysis shows that the ratio between the measured and ex-
 pected entropy scales as $\mathcal{S}(g)/\mathcal{S}_N \propto 1/N$. Similarly as observed
 above, the Shannon entropy may thus become ineffective in di-
 agnosing fission source convergence in the presence of spatial
 clustering.

230 One might wonder whether the results discussed in this Sec-
 tion are specific to exactly critical configurations (i.e., to hav-
 ing chosen $k_{\text{eff}} = 1$). Actually, this is not the case. We have
 performed several other Monte Carlo power iteration simula-
 tions for super- or sub-critical reactors by varying the system
 235 parameters, and the outcomes are qualitatively similar to those
 presented here. Finally, the behaviour of the entropy function
 with respect to the mesh number B is presented in Fig. 5. The
 convergence to the asymptotic value \mathcal{S}_N for any fixed N de-
 creases for increasing B , which is clearly understood on phys-
 240 ical grounds. Indeed, when the number of mesh B is larger,
 the number of particles N required to smooth out the effects
 of correlations in each spatial bin must be also larger. In par-
 ticular, we have numerically observed that we have the scaling
 $(\mathcal{S}_N - \mathcal{S}(g))/\mathcal{S}_N \propto B^{1/3}$ for fixed N and L .

245 3. Beyond entropy: extracting information from spatial moments

The main drawback of the entropy function as a tool for the
 250 statistical analysis of Monte Carlo power iteration is that the
 spatial fluctuations of the neutron population are somehow aver-
 aged out by the sum over all cells in Eq. 1: an asymptotic con-
 vergence can be ultimately attained even if neutrons are subject
 to strong (but statistically stationary in space) patchiness. Clus-
 255 tering effects will then go undetected when using the standard
 definition of $\mathcal{S}(g)$ during power iteration, unless the theoretical

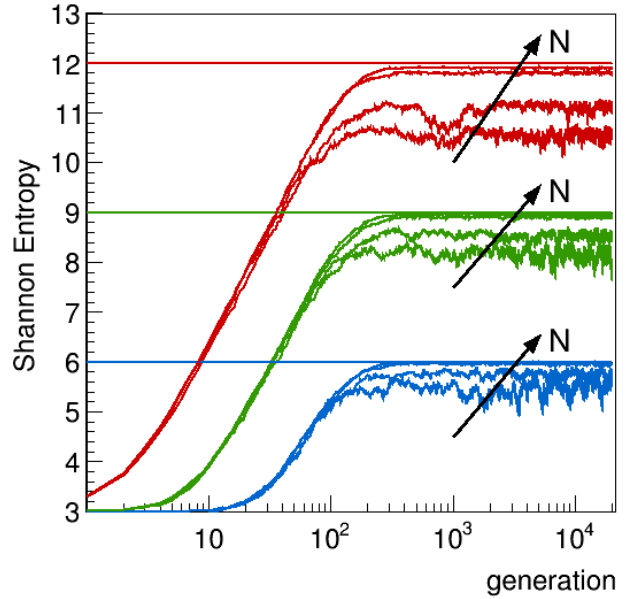


Figure 5: Homogeneous cube reactor. The behaviour of the
 measured Shannon entropy $\mathcal{S}(g)$ during Monte Carlo power iter-
 ation as a function of generations g , for different mesh num-
 ber B , and fixed $L = 400 \text{ cm}$. The guess source at $g = 0$ con-
 sists of N neutrons located at the center of the cube. Power
 iteration is run for 2×10^4 generations. Upper red curves:
 $B = 16 \times 16 \times 16$; central green curves: $B = 8 \times 8 \times 8$; lower
 blue curve: $B = 4 \times 4 \times 4$. For any fixed B , N is progressively
 increased, i.e., $N = 5 \times 10^3$, $N = 10^4$, $N = 5 \times 10^4$, $N = 10^5$.
 For reference, the corresponding theoretical entropy values \mathcal{S}_∞
 are displayed as solid lines.

value \mathcal{S}_N is known in advance, so that the ratio $\mathcal{S}(g)/\mathcal{S}_N$
 can be computed. Generally speaking, this is however not possible
 but for the simplest reactor configurations, such as the homoge-
 neous cube considered above.

In order to explicitly include the effects of spatial correla-
 tions in our statistical analysis, a convenient choice consists in
 generalizing the entropy function defined in Eq. 1 as follows:

$$260 \mathcal{S}_{u,v,w}^* = - \sum_{i,j,k} \mathcal{L}_u(\xi_i) \mathcal{L}_v(\xi_j) \mathcal{L}_w(\xi_k) p_{i,j,k} \log_2[p_{i,j,k}], \quad (7)$$

where $\mathcal{L}_q(\zeta)$ are the Legendre polynomials (other basis sets
 could also be used) of order q and argument ζ , and ξ_i is the
 x -coordinate (ξ_j is the y -coordinate, and ξ_k is the z -coordinate,
 respectively) of the center of the cell i, j, k , normalized to the
 interval $[-1, 1]$. When $u = v = w = 0$, we recover the regu-
 lar Shannon entropy function, namely, $\mathcal{S}_{0,0,0}^*(g) = \mathcal{S}(g)$. For
 $q = 1$, we have $\mathcal{L}_1(\zeta) = \zeta$, so that the quantity $\mathcal{S}_{1,0,0}^*(g)$ can
 be interpreted as the first spatial moment of the entropy function
 along the x direction ($\mathcal{S}_{0,1,0}^*(g)$ in the y direction and $\mathcal{S}_{0,0,1}^*(g)$
 in the z direction, respectively). In other words, the function $\mathcal{S}_{u,v,w}^*$
 weights the fluctuations in the number of particles at a cell i, j, k
 of the mesh along each spatial axis by the regular Shannon en-
 265 tropy defined on the same mesh.

By construction, the generalized entropy function $\mathcal{S}_{u,v,w}^*(g)$ is better suited than $\mathcal{S}(g)$ in detecting spatial fluctuations during the Monte Carlo power iteration. In order to illustrate our argument, let us revisit the homogeneous cubic reactor of the previous Section, with a fixed number of meshes $B = 512$. The behaviour of $\mathcal{S}_{1,0,0}^*(g)$ for the reactor configurations obtained by keeping the number of neutrons N fixed and varying the box size L is illustrated in Fig. 6 (top). The first spatial moment of the entropy along the x direction is expected to be zero due to the symmetry of neutron distribution. Since the source for the power iteration is initially placed at the center of the box, there is no appreciable convergence phase for $\mathcal{S}_{1,0,0}^*(g)$, as opposed to $\mathcal{S}(g)$. Fluctuations of $\mathcal{S}_{1,0,0}^*(g)$ around zero clearly mirror the spatial correlations: as L increases, correlations become stronger and the fluctuations of $\mathcal{S}_{1,0,0}^*(g)$ become wilder. A similar behaviour is found when decreasing the number N of simulated neutrons per generations at fixed reactor size L , as shown in Fig. 7 (top). When N is large, the $\mathcal{S}_{1,0,0}^*(g)$ is again close to zero, and the fluctuations increase by decreasing N . For symmetry reasons, the results for $\mathcal{S}_{0,1,0}^*(g)$ and $\mathcal{S}_{0,0,1}^*(g)$ are (statistically) identical to those obtained for $\mathcal{S}_{1,0,0}^*(g)$ and will thus not be shown here.

A second, and perhaps more intuitive, approach to the analysis of spatial fluctuations during power iteration consists in computing the center of mass $\mathbf{r}_{com}(g)$ of the neutrons as a function of generations g , as recently suggested for instance by (Wenner and Haghghat, 2007, 2008). To be more precise, for a collection of N particles having coordinates $\{x_1, y_1, z_1, \dots, x_N, y_N, z_N\}$ at the fission sites, the center of mass is defined as

$$\mathbf{r}_{com}(g) = \frac{\sum_i w_i \mathbf{r}_i}{\sum_i w_i}, \quad (8)$$

where \mathbf{r}_i is the vector of components $\mathbf{r}_i = \{x_i, y_i, z_i\}$, and w_i are the statistical weights of the neutrons. The components of the center of mass along each direction are defined as

$$x_{com}(g) = \frac{\sum_i w_i x_i}{\sum_i w_i}, \quad y_{com}(g) = \frac{\sum_i w_i y_i}{\sum_i w_i}, \quad z_{com}(g) = \frac{\sum_i w_i z_i}{\sum_i w_i}. \quad (9)$$

Observe that by construction the center of mass $\mathbf{r}_{com}(g)$ does not depend on the number of spatial meshes.

The analysis of the center of mass estimator for the reactor configurations obtained by keeping the number of neutrons N fixed and varying the box size L is illustrated in Fig. 6 (bottom), where we display $x_{com}(g)$. Since the source for the power iteration is initially placed at the center of the box, there is no appreciable convergence phase for $x_{com}(g)$. The evolution of $x_{com}(g)$ clearly mirrors the spatial fluctuations of the neutron population: when L is small, and the population is uniformly distributed within the box, $x_{com}(g)$ fluctuates around the symmetry center (here, $x = y = z = 0$), and the fluctuations are rather mild. As L increases, the effects of spatial correlations becomes stronger, and the evolution of $x_{com}(g)$ becomes increasingly erratic. The qualitative behaviour of $x_{com}(g)$ is closely related to that of $\mathcal{S}_{1,0,0}^*(g)$, apart from the normalizing factor that is imposed by construction in the Legendre polynomials for $\mathcal{S}_{u,v,w}^*(g)$.

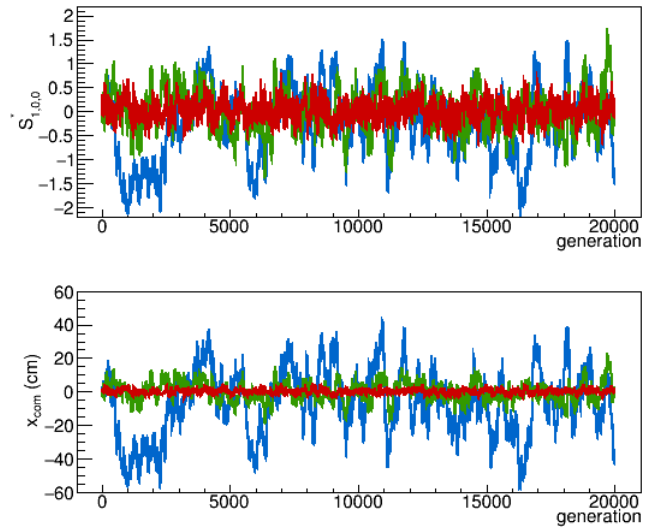


Figure 6: Homogeneous cube reactor. Monte Carlo power iteration as a function of generations g , for three different reactor sizes L and fixed number N of neutrons per generation. The guess source at $g = 0$ consists of $N = 10^4$ neutrons located at the center of the cube. Power iteration is run for 1000 generations. Top. The behaviour of the generalized Shannon entropy $\mathcal{S}_{1,0,0}^*(g)$. Red curve: $L = 100$ cm; Green curve: $L = 200$ cm; Blue curve: $L = 400$ cm. Bottom. The behaviour of the center of mass $x_{com}(g)$. Red curve: $L = 100$ cm; Green curve: $L = 200$ cm; Blue curve: $L = 400$ cm.

A similar behaviour is again found for $x_{com}(g)$ when decreasing the number N of simulated neutrons per generations at fixed reactor size L , as shown in Fig. 7 (bottom). The fluctuations of $x_{com}(g)$ increase by decreasing N , and the qualitative evolution of $x_{com}(g)$ is strikingly similar to that of $\mathcal{S}_{1,0,0}^*(g)$. For symmetry reasons, the results for $y_{com}(g)$ and $z_{com}(g)$ are (statistically) identical to those obtained for $x_{com}(g)$ and will thus not be shown here.

4. The impact of clustering on the spatial moments

A deeper understanding of the qualitative behaviour of the generalized entropy and by the center of mass that we have observed in the previous Section can be achieved by relating the features of these estimators to the key physical parameters that govern the evolution of the Monte Carlo power iteration. This is actually possible by resorting to the theory of branching stochastic processes. Since the features of the generalized entropy are almost identical to those of the center of mass, for our analysis in the following we will focus on this latter.

The nuclear reactor model described above can be conceptually represented as a collection of N particles undergoing scattering, reproduction and absorption within a homogeneous box of finite volume V , with reflecting (mass-preserving) boundaries. In order to keep notation simple, and yet retain the key ingredients of the model, we will approximate the exponential

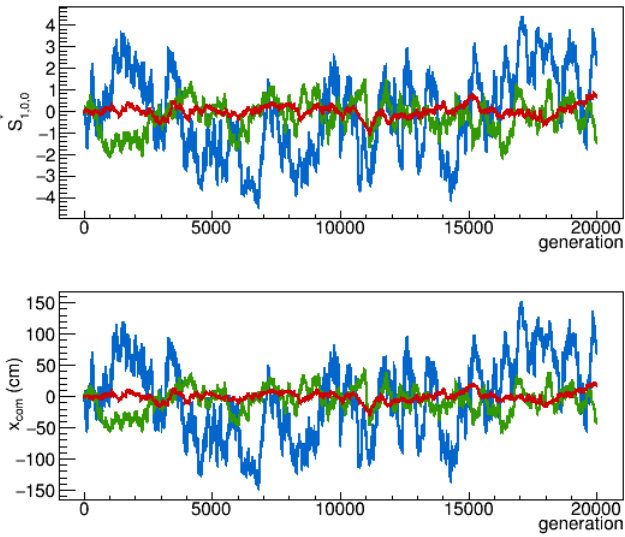


Figure 7: Homogeneous cube reactor. Monte Carlo power iteration as a function of generations g , for three different initial population sizes N and fixed $L = 400$ cm. The guess source at $g = 0$ consists of N neutrons located at the center of the cube. Power iteration is run for 1000 generations. Top. The behaviour of the generalized Shannon entropy $\mathcal{S}_{1,0,0}^*(g)$. Red curve: $N = 10^5$; green curve: $N = 10^4$; blue curve: $N = 10^3$. Bottom. The behaviour of the center of mass $x_{com}(g)$. Red curve: $N = 10^5$; green curve: $N = 10^4$; blue curve: $N = 10^3$.

paths of the neutrons by regular Brownian motion with a constant diffusion coefficient D (in other words, we are assuming that the diffusion approximation holds). For the same reason, instead of working with discrete generations we will introduce a continuous time t . The diffusing walker undergoes a birth-death event at rate $\beta = \nu\Sigma_f$: the neutron disappears and is replaced by a random number k of descendants, distributed according to a law q_k with average $\bar{\nu}_f = \sum_k kq_k$. We will assume that exactly two neutrons are emitted at fission.

In the Monte Carlo power iteration, some population control mechanisms are typically applied (such as Russian roulette and splitting), and the neutron population is typically normalized at the end of each generation in order to prevent the number of individuals from either exploding or shrinking to zero. For our aims, the effect of such population control mechanisms on our model can be mimicked by imposing that the total number N of neutrons in V is preserved. The simplest way to ensure a constant N is to correlate fission and capture events (Zhang et al., 1990; Meyer et al., 1996): at each fission, a neutron disappears and is replaced by 2 descendants, and 1 neutron is simultaneously captured (i.e., removed from the collection) in order to ensure the conservation of total population².

²This mechanism has been first introduced in the theoretical ecology (Zhang et al., 1990; Meyer et al., 1996), where similar large-scale constraints have been shown to quench the wild fluctuations in the number of individuals that are expected for an unconstrained community.

Analysis of this model shows that the evolution of the neutron population is governed by two distinct time scales: a mixing time $\tau_D \propto V^{2/3}/D$ and a renewal time $\tau_R \propto N/\beta$. The quantity τ_D physically represents the time over which a particle has explored the finite viable volume V by diffusion. The emergence of the time scale τ_D is a distinct feature of confined geometries having a finite spatial size: for unbounded domains, $\tau_D \rightarrow \infty$. The quantity τ_R represents the time over which the system has undergone a population renewal, and all the individuals descend from a single common ancestor. When the concentration N/V of individuals in the population is large (and the system is spatially bounded), it is reasonable to assume that $\tau_R > \tau_D$.

Consider then a collection of N such particles moving around randomly, whose vector positions $\mathbf{r}_i(t)$, $i = 1, \dots, N$, are recorded at time t . The spatial behaviour of the individuals can be characterized in terms of several moments, namely, the square center of mass

$$\langle \mathbf{r}_{com}^2 \rangle(t) \equiv \left\langle \left(\frac{1}{N} \sum_i \mathbf{r}_i(t) \right)^2 \right\rangle, \quad (10)$$

the mean square displacement

$$\langle \mathbf{r}^2 \rangle(t) \equiv \frac{1}{N} \sum_i \langle \mathbf{r}_i^2(t) \rangle, \quad (11)$$

and the mean square distance between pairs of particles

$$\langle \mathbf{r}_p^2 \rangle(t) \equiv \frac{1}{N(N-1)} \sum_{i,j} \langle |\mathbf{r}_i(t) - \mathbf{r}_j(t)|^2 \rangle. \quad (12)$$

Brackets denote the expectation with respect to the ensemble of possible realizations.

By construction, these three quantities are related to each other. By developing the series in the definitions above, we can in particular express the center of mass as a function of the mean square displacement and of the particle pair distance (Meyer et al., 1996), namely,

$$\langle \mathbf{r}_{com}^2 \rangle(t) = \langle \mathbf{r}^2 \rangle(t) - \frac{1}{2} \frac{N-1}{N} \langle \mathbf{r}_p^2 \rangle(t). \quad (13)$$

In the following, we will explicitly compute the center of mass for the homogeneous reactor and relate its behaviour to the model parameters.

4.1. Neutron density and correlations

Let us denote by $n(\mathbf{x}, t)$ the instantaneous density of neutrons located at \mathbf{x} at time t . For a critical reactor, the average neutron density at a point \mathbf{x} reads

$$\langle n(\mathbf{x}, t) \rangle = N\rho(\mathbf{x}_i, t), \quad (14)$$

where we have set

$$\rho(\mathbf{x}, t) = \int d\mathbf{x}_0 \mathcal{Q}(\mathbf{x}_0) \mathcal{G}(\mathbf{x}, \mathbf{x}_0, t). \quad (15)$$

Here Q is the spatial probability distribution function of the neutrons at time $t = 0$, and the Green's function $\mathcal{G}(\mathbf{x}, \mathbf{x}_0, t)$ satisfies the backward diffusion equation

$$\frac{\partial}{\partial t} \mathcal{G}(\mathbf{x}, \mathbf{x}_0, t) = D \nabla_{\mathbf{x}_0}^2 \mathcal{G}(\mathbf{x}, \mathbf{x}_0, t), \quad (16)$$

with the appropriate boundary conditions (de Mulatier et al., 2015). Assuming that the initial neutron population has a uniform spatial distribution, we have $Q = 1/V$, and the average neutron density at any time will be spatially uniform, namely, $\langle n(\mathbf{x}, t) \rangle = N/V$. For arbitrarily distributed sources at $t = 0$, the neutron density will asymptotically converge towards $\langle n(\mathbf{x}, t \rightarrow \infty) \rangle = N/V$ for long times.

The spatial inhomogeneities of the neutron population due to clustering can be probed by resorting to the pair correlation function $h(\mathbf{x}, \mathbf{y}, t)$ between positions \mathbf{x} and \mathbf{y} , namely, the average density of pairs with the former particle in \mathbf{x} and the latter in \mathbf{y} (de Mulatier et al., 2015). This quantity is proportional to the joint probability density for \mathbf{x} and \mathbf{y} (Meyer et al., 1996). The spatial shape of $h(\mathbf{x}, \mathbf{y}, t)$ conveys information on the correlation range, whereas its amplitude is proportional to the correlation strength. A flat shape implies that the correlations have the same intensity everywhere; on the contrary, the presence of a peak at $\mathbf{x} \simeq \mathbf{y}$ reflects the increased probability of finding particles at short distances of each other, which is the signature of spatial clustering (Zhang et al., 1990; Meyer et al., 1996). For the ideal case of N independent random walkers in the absence of branching and death we would have

$$h_{id}(\mathbf{x}, \mathbf{y}, t) = N(N-1)\rho(\mathbf{x}, t)\rho(\mathbf{y}, t). \quad (17)$$

In particular, if the particles are uniformly distributed at time $t = 0$, $h_{id}(\mathbf{x}, \mathbf{y}, t) = N(N-1)/V^2$.

For the homogeneous reactor model defined above, the pair correlation function h can be exactly computed by resorting to the approach originally proposed in (Meyer et al., 1996) for infinite domains and later refined by (de Mulatier et al., 2015) for bounded domains. The calculations are developed in Appendix B, and yield

$$h(\mathbf{x}, \mathbf{y}, t) = \frac{N(N-1)}{V^2} e^{-\beta_p t} + \beta \frac{N}{V} \int_0^t dt' e^{-\beta_p t'} \mathcal{G}(\mathbf{x}, \mathbf{y}, 2t') \quad (18)$$

when imposing the initial uniform source $Q = 1/V$. The quantity β_p is a shorthand for $\beta_p = \beta/(N-1)$. When branching events are absent ($\beta = 0$), $h(\mathbf{x}, \mathbf{y}, t) \rightarrow h_{id}(\mathbf{x}, \mathbf{y}, t)$, since spatial correlations are suppressed. The integral of the Green's function appearing in Eq. 18 is bounded thanks to the exponential term, and at long times the correlation function converges to an asymptotic shape. The same asymptotic behaviour is expected for arbitrary initial sources.

4.2. Relating the spatial moments to ρ and h

The spatial moments of the neutron population defined above can be formally expressed in terms of the particle density $\rho(\mathbf{x}, t)$

and of the correlation function $h(\mathbf{x}, \mathbf{y}, t)$. In particular, for the mean square displacement we have

$$\langle \mathbf{r}^2 \rangle(t) = \int \mathbf{x}^2 \rho(\mathbf{x}, t) d\mathbf{x}. \quad (19)$$

As for the mean square distance between pairs of particles, we have

$$\langle \mathbf{r}_p^2 \rangle(t) = \frac{\int d\mathbf{x} \int d\mathbf{y} |\mathbf{x} - \mathbf{y}|^2 h(\mathbf{x}, \mathbf{y}, t)}{\int d\mathbf{x} \int d\mathbf{y} h(\mathbf{x}, \mathbf{y}, t)}, \quad (20)$$

which is to be compared to the ideal average square distance of an uncorrelated population uniformly distributed in the viable volume, namely,

$$\langle \mathbf{r}_p^2 \rangle_{id} = \frac{1}{V^2} \int d\mathbf{x} \int d\mathbf{y} |\mathbf{x} - \mathbf{y}|^2 = \frac{1}{2} V^{\frac{3}{3}}. \quad (21)$$

Deviations of $\langle \mathbf{r}_p^2 \rangle(t)$ from the ideal behaviour $\langle \mathbf{r}_p^2 \rangle_{id}$ allow quantifying the impact of spatial clustering (Meyer et al., 1996; de Mulatier et al., 2015).

4.3. Analysis of the homogeneous reactor

Let us now consider the case of the homogeneous cube reactor introduced above, with size L and $V = L^3$. At the boundaries, we impose reflecting (Neumann) conditions. The Green's function for this system reads (Grebekov, 2013)

$$\mathcal{G}(\mathbf{x}, \mathbf{x}_0, t) = \sum_{i,j,k} \varphi_i(u) \varphi_i^\dagger(u_0) \varphi_j(v) \varphi_j^\dagger(v_0) \varphi_k(w) \varphi_k^\dagger(w_0) e^{-\alpha_{i,j,k} t},$$

where

$$\varphi_q(\zeta) = \cos\left(\frac{q\pi\zeta}{L}\right) \quad (22)$$

are the eigen-modes of the Laplace operator and

$$\alpha_{i,j,k} = D \left(\frac{\pi}{L}\right)^2 (i^2 + j^2 + k^2) \quad (23)$$

are the associated eigenvalues. The vector \mathbf{x} is defined by its components, namely, $\mathbf{x} = \{u, v, w\}$. By inspection, the mixing time of the neutron population is identified with $\tau_D \propto L^2/(\pi^2 D)$. The functions $\varphi_q^\dagger(\zeta)$ are found by imposing ortho-normalization of the eigenmodes, which yields

$$\varphi_q^\dagger(\zeta) = \frac{1}{L} \cos\left(\frac{q\pi\zeta}{L}\right) \quad (24)$$

for $q = 0$, and

$$\varphi_q^\dagger(\zeta) = \frac{2}{L} \cos\left(\frac{q\pi\zeta}{L}\right) \quad (25)$$

for $q \geq 1$.

Assuming a uniform spatial distribution $Q = 1/L^3$ at time $t = 0$, the average density simply reads

$$\langle n(\mathbf{x}, t) \rangle = \frac{N}{L^3}. \quad (26)$$

The mean square displacement can be easily computed, and yields

$$\langle \mathbf{r}^2 \rangle(t) = \int \mathbf{x}^2 \rho(\mathbf{x}, t) d\mathbf{x} = \frac{L^2}{4}. \quad (27)$$

From Eq. 18 we get the pair correlation function

$$h(\mathbf{x}, \mathbf{y}, t) = \frac{N(N-1)}{L^6} + \beta N \sum_{i', j', k'} \varphi_i(u) \varphi_i^\dagger(q) \varphi_j(v) \varphi_j^\dagger(r) \varphi_k(w) \varphi_k^\dagger(s) \frac{1 - e^{-(2\alpha_{i,j,k} + \beta_p)t}}{2\alpha_{i,j,k} + \beta_p},$$

where the sum is extended to all indexes $i \geq 0, j \geq 0, k \geq 0$, except $i = j = k = 0$, and we have set $\mathbf{x} = \{u, v, w\}$ and $\mathbf{y} = \{p, r, s\}$. The series appearing at the right-hand side is bounded, and for times $t \gg \tau_D$ we obtain the asymptotic shape of the pair correlation function

$$h_\infty(\mathbf{x}, \mathbf{y}) = \frac{N(N-1)}{L^6} + \beta N \sum_{i', j', k'} \frac{\varphi_i(u) \varphi_i^\dagger(q) \varphi_j(v) \varphi_j^\dagger(r) \varphi_k(w) \varphi_k^\dagger(s)}{2\alpha_{i,j,k} + \beta_p}. \quad (28)$$

As for the average square distance, at time $t = 0$ we have $\langle \mathbf{r}_p^2 \rangle(0) = \langle \mathbf{r}_p^2 \rangle_{id}$, as expected. The asymptotic behaviour of $\langle \mathbf{r}_p^2 \rangle(t)$ at times $t \gg \tau_D$ can be computed exactly based on Eqs. (28) and (20), and reads

$$\langle \mathbf{r}_p^2 \rangle_\infty = \lim_{t \rightarrow \infty} \langle \mathbf{r}_p^2 \rangle(t) = 12 \frac{D}{\beta_p} \left[1 - \sqrt{\frac{8D}{\beta_p L^2}} \tanh \left(\sqrt{\frac{\beta_p L^2}{8D}} \right) \right]. \quad (29)$$

By recalling the definitions of the mixing time τ_D and the renewal time τ_R , we can rewrite Eq. (29) as

$$\langle \mathbf{r}_p^2 \rangle_\infty = \frac{12L^2}{\pi^2} \frac{\tau_R}{\tau_D} \left[1 - \sqrt{\frac{8}{\pi^2} \frac{\tau_R}{\tau_D}} \tanh \left(\sqrt{\frac{\pi^2}{8} \frac{\tau_D}{\tau_R}} \right) \right], \quad (30)$$

which shows that the impact of the spatial correlations is ruled by the dimensionless ratio between the renewal time and the mixing time. Intuitively, we expect the effects of the correlations to be stronger when the typical time scale of fission renewal is in competition with diffusive mixing (i.e., $\tau_R \approx \tau_D$), and to be weaker when diffusive mixing is faster than renewal (i.e., $\tau_D \ll \tau_R$).

Let us first consider the case of a system where the effects of the spatial correlations induced by clustering are very weak (i.e., $\tau_R \rightarrow \infty$), which is obtained for a very large number of particles or a vanishing fission rate. By taking the limit of $\beta \rightarrow 0$ or equivalently $N \rightarrow \infty$, we have

$$\langle \mathbf{r}_p^2 \rangle \rightarrow \frac{L^2}{2} = \langle \mathbf{r}_p^2 \rangle_{id} \quad (31)$$

and we recover the ideal case corresponding to uncorrelated trajectories. In this case, the center of mass of the population obeys

$$\langle \mathbf{r}_{com}^2 \rangle_{id} = \langle \mathbf{r}^2 \rangle - \frac{1}{2} \frac{N-1}{N} \langle \mathbf{r}_p^2 \rangle_{id} = \frac{L^2}{4N} = \frac{1}{N} \langle \mathbf{r}^2 \rangle_{id}, \quad (32)$$

which basically means that for a collection of independent particles the mean square displacement of the center of mass is

equal to the mean square displacement of a single particle of the collection, divided by the number of particles.

Consider now a finite reproduction rate β and a large but finite number of particles $N \gg 1$. In this case, we can expand Eq. (30) for $\tau_D \ll \tau_R$, which yields

$$\begin{aligned} \langle \mathbf{r}_p^2 \rangle_\infty &\approx \frac{L^2}{2} \left[1 - \frac{\pi^2}{20} \frac{\tau_D}{\tau_R} + \dots \right] \\ &= \langle \mathbf{r}_p^2 \rangle_{id} \left[1 - \frac{1}{20} \frac{L^2}{N \mathcal{M}^2} + \dots \right], \end{aligned} \quad (33)$$

where we have used the definition of the migration area $\mathcal{M}^2 = D/\beta$. This result relates the typical inter-particle distance to the physical parameters of the reactor model, namely, N , L , and \mathcal{M}^2 , and implies in particular that $\langle \mathbf{r}_p^2 \rangle_\infty$ will be smaller than in the uncorrelated case because of the effects of spatial clustering.

As for the center of mass, we finally get

$$\begin{aligned} \langle \mathbf{r}_{com}^2 \rangle_\infty &= \langle \mathbf{r}^2 \rangle - \frac{1}{2} \frac{N-1}{N} \langle \mathbf{r}_p^2 \rangle_\infty \approx \frac{L^2}{4N} \left[1 + \frac{\pi^2}{20} N \frac{\tau_D}{\tau_R} + \dots \right] \\ &= \langle \mathbf{r}_{com}^2 \rangle_{id} \left[1 + \frac{1}{20} \frac{L^2}{\mathcal{M}^2} + \dots \right], \end{aligned} \quad (34)$$

which again relates the mean square displacement of the center of mass to the physical parameters N , L , and \mathcal{M}^2 . In particular, $\langle \mathbf{r}_{com}^2 \rangle_\infty$ will be larger than that of an uncorrelated system. The correction factor increases for increasing system size L , and decreases for increasing migration area \mathcal{M}^2 , as expected on physical grounds.

4.4. Numerical findings for the homogeneous reactor

It is interesting to compare the numerical values of $\langle \mathbf{r}_{com}^2 \rangle_\infty$ predicted by Eq. (34) to the behaviour of the center of mass displayed in Fig. 6 (bottom) and Fig. 7 (bottom). In particular, $\sigma_{com} = \sqrt{\langle \mathbf{r}_{com}^2 \rangle_\infty}$ intuitively represents the typical amplitude of the fluctuations of the center of mass around the average. The value of \mathcal{M}^2 can be estimated by computing ℓ^2 in each Monte Carlo simulation and then setting $\mathcal{M}^2 = \ell^2/6$ according to diffusion theory. Because of the geometrical symmetries of the cube configuration, along a given axis, say x , we get $\sigma_{com}^x = \sqrt{\langle \mathbf{r}_{com}^2 \rangle_\infty}/3$.

When the number of particles is kept fixed at $N = 10^4$, and the size L varies, from Eq. (34) we get for σ_{com}^x the values reported in Tab. 1. These findings are entirely consistent with the typical size of the fluctuations of the x component of the center of mass observed in Fig. 6 (bottom): for comparison, the standard deviation $\hat{\sigma}_{com}^x$ of the recorded statistical series is also reported in Tab. 1.

When the reactor size is kept fixed at $L = 400$ cm ($\ell^2 \approx 192$ cm²) and N varies, from Eq. (34) we get the σ_{com}^x values reported in Tab. 2. Comparison with Fig. 7 (bottom) shows that these predictions are again entirely consistent with the typical size of the fluctuations of the x component of the center of mass observed in our Monte Carlo simulations, whose standard deviation $\hat{\sigma}_{com}^x$ is also reported in Tab. 2.

L [cm]	ℓ^2 [cm ²]	σ_{com}^x [cm]	$\hat{\sigma}_{com}^x$ [cm]
100	174	1.2	1.5
200	185	4.7	5.9
400	192	18.3	19.9

Table 1: Measured and predicted values for the fluctuations of the x component of the center of mass for the homogeneous cube reactor. Here the number of neutrons per generation is kept fixed at $N = 10^4$, and the reactor size L varies.

N	σ_{com}^x [cm]	$\hat{\sigma}_{com}^x$ [cm]
10^5	5.8	7.3
10^4	18.3	19.9
10^3	57.8	64.4

Table 2: Measured and predicted values for the fluctuations of the x component of the center of mass for the homogeneous cube reactor. Here the reactor size L is kept fixed at $L = 400$ cm, and the number N of neutrons per generation varies.

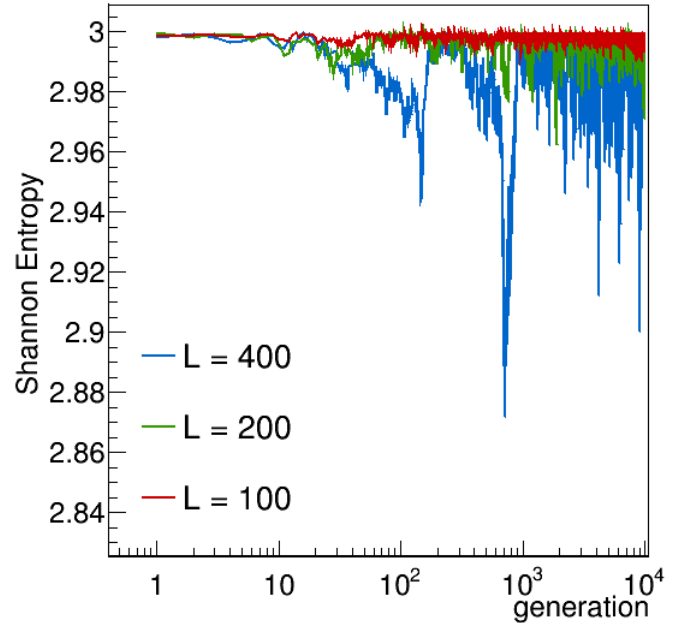


Figure 8: The fuel rod. The behaviour of the measured Shannon entropy $\mathcal{S}(g)$ during Monte Carlo power iteration as a function of generations g , for three different fuel rod lengths L and fixed number N of neutrons per generation. The guess source at $g = 0$ consists of $N = 10^4$ neutrons uniformly distributed along the fuel rod. Power iteration is run for 2×10^4 generations. Upper red curve: $L = 100$ cm; central green curve: $L = 200$ cm; lower blue curve: $L = 400$ cm. The mesh chosen for the entropy computation is fixed to 8 identical meshes along the total length of the fuel rod. The theoretical value of the entropy given by Eq. (5) reads $\mathcal{S}_\infty = 3.0$.

5. Application to realistic reactor configurations

In the previous Sections, we have applied our analysis to a simplified reactor model. In the following, we would like to ascertain whether the conclusions that were drawn in the case of space- and energy-independent neutron transport actually carry over to more realistic configurations. To this aim, we will examine the behaviour of Monte Carlo power iteration for a fuel rod and for a full reactor core. Monte Carlo simulations have been performed by resorting to the reference code TRIPOLI-4[®], developed at CEA (Brun et al., 2014; TRIPOLI-4 Project Team, 2008).

5.1. A fuel rod

Let us begin by considering a fuel rod. This configuration is composed of UO₂ fuel at 3.25% enrichment, with radius 0.407 cm. The fuel pellets are enclosed in a Zircaloy cladding of outer radius 0.477 cm, and a water moderator surrounds the cladding. All materials are kept at 300 K. Reflective boundary conditions have been applied on the system, so that the expected equilibrium distribution for the flux is axially flat in space. The chosen nuclear data library is ENDF/B-VII.0.

The measured entropy function $\mathcal{S}(g)$ for the fuel rod is shown in Fig. 8 for fixed number N of simulated particles per generation and varying fuel rod sizes L , and in Fig. 9 for fixed L and varying N , respectively. When L is varied and $N = 10^4$, the entropy function converges to a stationary value after about $m = L^2/\ell^2 \simeq 100$ generations for $L = 100$ cm ($\ell^2 \simeq 100$ cm²), $m = L^2/\ell^2 \simeq 370$ generations for $L = 200$ cm ($\ell^2 \simeq 108$ cm²), and $m = L^2/\ell^2 \simeq 1400$ generations for $L = 400$ cm ($\ell^2 \simeq 112$ cm²). Our predictions are consistent with the numerical findings for $\mathcal{S}(g)$. The entropy at convergence depends on the number N of simulated particles per generations, and an asymptotic value \mathcal{S}_N is eventually reached in the limit of large N , with a $\propto 1/N$ scaling.

The behaviour of $\mathcal{S}_{0,0,1}^*(g)$ for the fuel rod with fixed N fixed and varying L is illustrated in Fig. 10 (top), z being the axis aligned along the rod. As L increases, the fluctuations of $\mathcal{S}_{0,0,1}^*(g)$ become stronger. A similar behaviour is found when decreasing the number N of simulated neutrons per generations at fixed reactor size L , as shown in Fig. 11 (top): the fluctuations increase by decreasing N . The analysis of the center of mass estimator for the fuel rod with fixed N and varying L is illustrated in Fig. 10 (bottom), where we display $z_{com}(g)$: when L is small, $z_{com}(g)$ fluctuates around the symmetry center $z = 0$, and the fluctuations are rather mild. As L increases, the evolution of $z_{com}(g)$ becomes increasingly erratic. The qualitative behaviour of $z_{com}(g)$ is similar to that of $\mathcal{S}_{0,0,1}^*(g)$. A similar behaviour is found for fixed L and varying N , as shown in Fig. 11 (bottom).

In order to relate the numerical simulation results for $z_{com}(g)$ to the theory developed above, we have solved Eq. (18) for a one-dimensional homogeneous rod geometry, where neutrons are allowed to only move back and forth along a line of size L . Neumann boundary conditions are applied to the ends of the

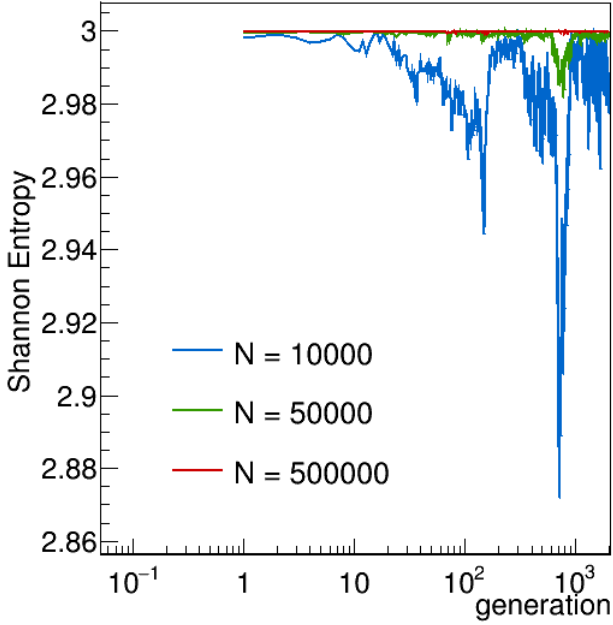


Figure 9: The fuel rod. The behaviour of the measured Shannon entropy $\mathcal{S}(g)$ during Monte Carlo power iteration as a function of generations g , for a fixed fuel cell length $L = 400$ cm and different numbers N of neutrons per generation. The guess source at $g = 0$ consists of N neutrons uniformly distributed along the fuel pin. Power iteration is run for 8×10^3 generations. Upper red curve: $N = 5 \times 10^5$; central green curve: $N = 5 \times 10^4$; lower blue curve: $N = 10^4$. The mesh chosen for the entropy computation is fixed to 8 identical meshes along the total length of the fuel rod. The theoretical value of the entropy given by Eq. (5) reads $\mathcal{S}_\infty = 3.0$.

segment. The rod model equations yield

$$\langle \mathbf{z}_{com}^2 \rangle_\infty = \langle \mathbf{z}_{com}^2 \rangle_{id} \left[1 + \frac{1}{20} \frac{L^2}{\mathcal{M}^2} + \dots \right], \quad (35)$$

with $\langle \mathbf{z}_{com}^2 \rangle_{id} = L^2/(12N)$ and $\mathcal{M}^2 = \ell^2/2$. For the case of fixed $N = 10^4$ and varying L , the rod model formula yields the σ_{com}^z values reported in Tab. 3. Comparison with Fig. 10 (bottom) shows that these predictions are in good agreement with the standard deviation $\hat{\sigma}_{com}^z$ of the recorded statistical series, which is also reported in Tab. 3.

L [cm]	ℓ^2 [cm ²]	σ_{com}^z [cm]	$\hat{\sigma}_{com}^z$ [cm]
100	100	1	0.9
200	108	2.6	3.3
400	112	13.8	15.4

Table 3: Measured and predicted values for the fluctuations of the z component of the center of mass for the fuel rod. Here the number of neutrons per generation is kept fixed at $N = 10^4$, and the fuel rod size L varies.

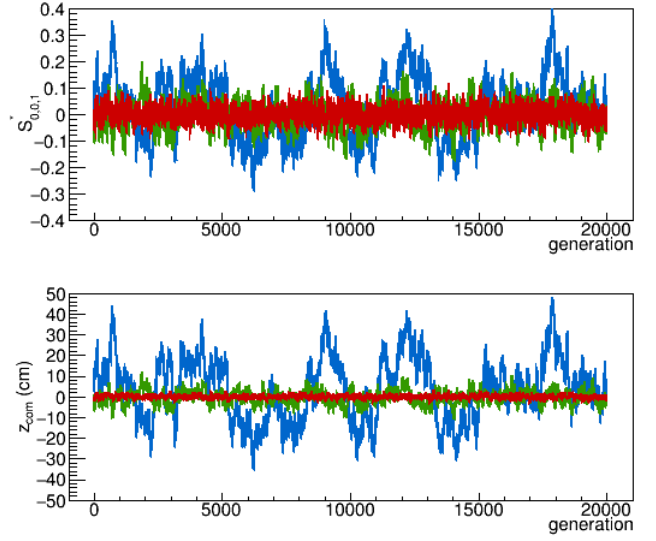


Figure 10: The fuel rod. Monte Carlo power iteration as a function of generations g , for three different reactor sizes L and fixed number N of neutrons per generation. The guess source at $g = 0$ consists of $N = 10^4$ neutrons uniformly distributed along the fuel rod. Power iteration is run for 2×10^4 generations. Top. The behaviour of the generalized Shannon entropy $\mathcal{S}_{0,0,1}^*(g)$. Red curve: $L = 100$ cm; Green curve: $L = 200$ cm; Blue curve: $L = 400$ cm. Bottom. The behaviour of the center of mass $z_{com}(g)$. Red curve: $L = 100$ cm; Green curve: $L = 200$ cm; Blue curve: $L = 400$ cm.

When $L = 400$ cm and N is varied, Eq. (35) yields the σ_{com}^z values reported in Tab. 4. These predictions are again in good agreement with the standard deviation $\hat{\sigma}_{com}^z$ of the recorded statistical series shown in Fig. 11 (bottom), which is also reported in Tab. 4.

N	σ_{com}^z [cm]	$\hat{\sigma}_{com}^z$ [cm]
10^5	2	1.7
5×10^4	6.2	4.9
10^4	13.8	15.4

Table 4: Measured and predicted values for the fluctuations of the z component of the center of mass for the fuel rod. Here the fuel rod size L is kept fixed at $L = 400$ cm, and the number N of neutrons per generation varies.

5.2. The Hoogenboom-Martin benchmark

Let us now turn our attention to a full-scale reactor core model, namely, the Hoogenboom-Martin benchmark (Hoogenboom and Martin, 2009). This benchmark considers a simplified PWR core made of 241 identical fuel assemblies. The fuel composition is representative of a typical depleted core configuration. Two moderator zones are used so as to model the decreasing bottom to top coolant density. We will focus on the

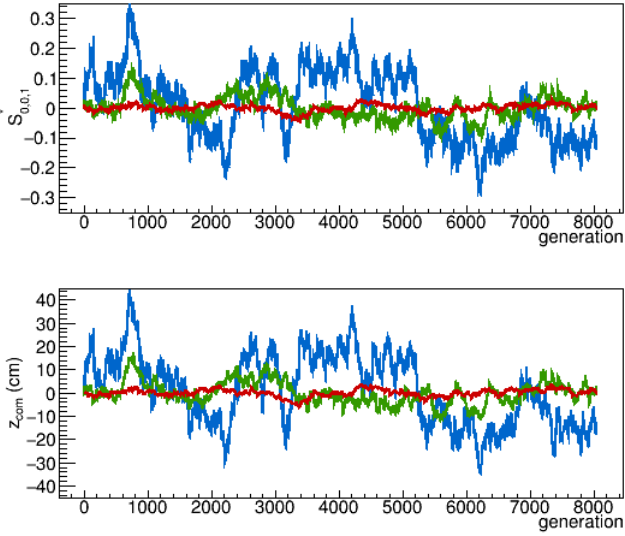


Figure 11: The fuel rod. Monte Carlo power iteration as a function of generations g , for a fixed fuel length $L = 400\text{cm}$ and different numbers N of neutrons per generation. The guess source at $g = 0$ consists of N neutrons uniformly distributed along the fuel rod. Power iteration is run for 8×10^3 generations. Top. The behaviour of the generalized Shannon entropy $S_{0,0,1}^*(g)$. Red curve: $N = 5 \times 10^5$; Green curve: $N = 5 \times 10^4$; Blue curve: $N = 10^4$. Bottom. The behaviour of the center of mass $z_{com}(g)$. Red curve: $N = 5 \times 10^5$; Green curve: $N = 5 \times 10^4$; Blue curve: $N = 10^4$.

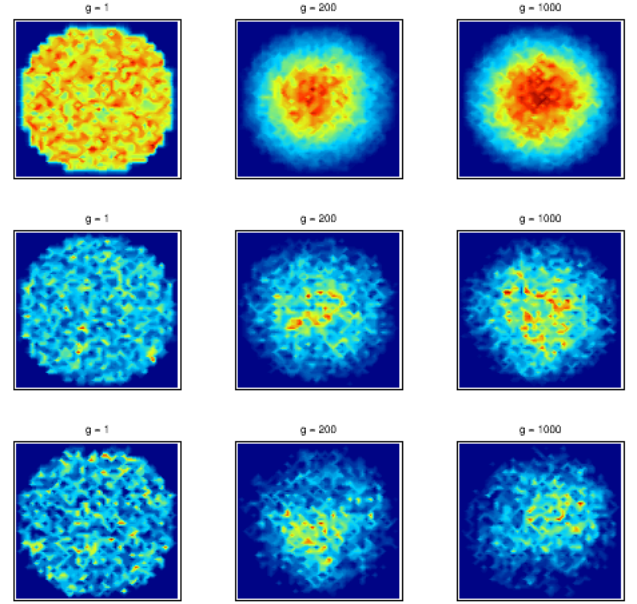


Figure 12: The Hoogenboom-Martin benchmark. Distribution of fission sites during Monte Carlo power iteration as a function of generations g , for three different initial population sizes N . The guess source at $g = 0$ consists of N neutrons uniformly distributed across the reactor. Power iteration is run for 12×10^4 generations. Top: $N = 10^5$; center: $N = 10^4$; bottom: $N = 5 \times 10^3$.

cold zero power core configuration (CZP: all materials are at room temperature, 300 K), and the chosen nuclear data library is ENDF/B-VII.0 (Chadwick et al., 2006).

By analogy with the simulations that were carried out for the homogeneous cube reactor, we will first examine the evolution of the fission site distribution as a function of the number of generations, for different values N of simulated neutrons per generation. The results for an axial cut at mid-plane are displayed in Fig. 12. We have chosen a uniform neutron source at $g = 0$. When $N = 10^5$, the population evolves toward the fundamental eigenmode, and the fluctuations around the average density are rather mild. When N decreases to $N = 10^4$, the impact of spatial correlations becomes stronger, and for even smaller $N = 5 \times 10^3$ neutrons are clearly clustered. Apart from geometrical effects due to the shape of the reactor core, the behaviour of the Monte Carlo power iteration of the Hoogenboom-Martin reactor model is not entirely dissimilar to that of the homogeneous cube.

The corresponding entropy function $S(g)$ is shown in Fig. 13. The mean square displacement per generation has been estimated within the Monte Carlo power iteration and reads $\ell^2 \simeq 356 \text{ cm}^2$. Similarly as in the case of the homogeneous cube reactor, the entropy function converges to a stationary value after about $m = H^2/\ell^2 \simeq 380$ generations, where we have used a characteristic reactor size $H \simeq 366 \text{ cm}$ corresponding to the active fuel length (and approximately to the core diameter). The

entropy at convergence depends on the number N of simulated particles per generations, and an asymptotic value S_N is eventually reached in the limit of large N , with a $\propto 1/N$ scaling.

N	σ_{com}^z [cm]	$\hat{\sigma}_{com}^z$ [cm]
10^5	3.5	1.8
5×10^4	5	2.2
10^4	11.3	5.8
5×10^3	15.9	8.6

Table 5: Measured and predicted values for the fluctuations of the z component of the center of mass for the Hoogenboom-Martin benchmark. The number N of neutrons per generation varies.

The behaviour of the spatial moments of the entropy function and of the center of mass for the Hoogenboom-Martin benchmark are displayed in Fig. 14 (top) and (bottom), respectively. When N is large, the $S_{0,0,1}^*(g)$ is close to zero, and the fluctuations increase by decreasing N . Similar results are found for the x and y axis, although geometrical effects come into play due to the cylindrical symmetry. The fluctuations of $z_{com}(g)$ also increase by decreasing N , and the qualitative evolution of $z_{com}(g)$ is very close to that of $S_{0,0,1}^*(g)$. Equation (18) can be developed for a homogeneous cylinder with Neumann boundaries, which conceptually corresponds to assuming that the water reflector surrounding the reactor core acts as a perfect mirror for neu-

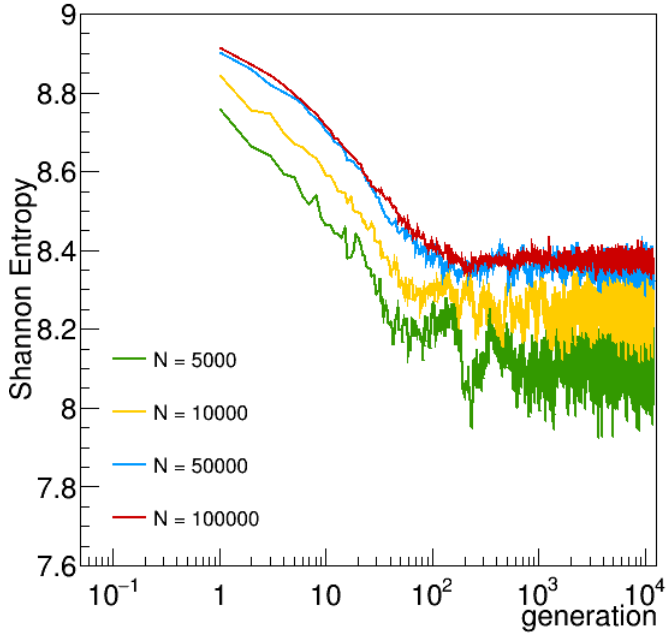


Figure 13: The Hoogenboom-Martin benchmark. The behaviour of the measured Shannon entropy $\mathcal{S}(g)$ during Monte Carlo power iteration as a function of generations g , for different initial population sizes N . The guess source at $g = 0$ consists of N neutrons uniformly distributed in the core. Power iteration is run for 12×10^4 generations. Upper red curve: $N = 10^5$; central green curve: $N = 10^4$; lower blue curve: $N = 5 \times 10^3$.

trons. In this case, for the z component of the center of mass fluctuations we would get

$$\langle \mathbf{z}_{com}^2 \rangle_{\infty} = \langle \mathbf{z}_{com}^2 \rangle_{id} \left[1 + \frac{1}{20} \frac{H^2}{\mathcal{M}^2} + \dots \right], \quad (36)_{565}$$

with $\langle \mathbf{z}_{com}^2 \rangle_{id} = H^2/(12N)$. Numerical estimates for σ_{com}^z are reported in Tab. 5, where we used $\mathcal{M}^2 = \ell^2/6 \simeq 60 \text{ cm}^2$. Comparison with Fig. 14 (bottom) shows that these predictions systematically overestimate (roughly by a factor of 2) the standard deviation $\hat{\sigma}_{com}^z$ of the recorded statistical series, which is also reported in Tab. 5.

Deviations of the theoretical formula in Eq. (34) from the observed behaviour of the fluctuations are mostly due to the approximation of entirely neglecting the effects of leakages in our simple model. Nonetheless, the order of magnitude of the fluctuation amplitude and the $1/\sqrt{N}$ scaling are correctly captured by Eq. (34).

6. Conclusions

The statistical behaviour of the neutrons in Monte Carlo power iteration has been analyzed within the framework of branching stochastic processes. In particular, we have shown that it is possible to relate the spatial distributions of neutrons to the key parameters of the simulated configuration, namely,

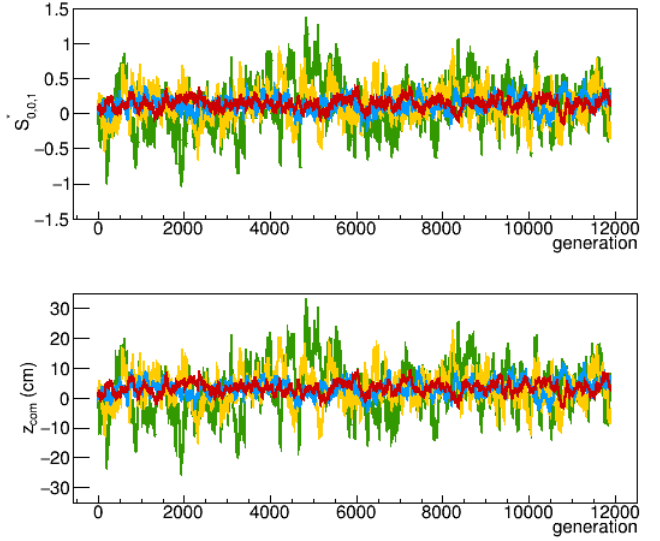


Figure 14: The Hoogenboom-Martin benchmark. Monte Carlo power iteration as a function of generations g , for three different initial population sizes N . The guess source at $g = 0$ consists of N neutrons located at the center of the cube. Power iteration is run for 12×10^4 generations. Top. The behaviour of the generalized Shannon entropy $\mathcal{S}_{0,0,1}^*(g)$. Red curve: $N = 10^5$; blue curve: $N = 5 \times 10^4$; yellow curve: $N = 10^4$; green curve: $N = 5 \times 10^3$. Bottom. The behaviour of the center of mass $z_{com}(g)$. Red curve: $N = 10^5$; blue curve: $N = 5 \times 10^4$; yellow curve: $N = 10^4$; green curve: $N = 5 \times 10^3$.

the number of neutrons per generation, the system size, and the migration area. By resorting to a simple homogeneous cube reactor model, we have illustrated some possible shortcomings of the entropy function in detecting the convergence of the neutron population to equilibrium. Alternative functions, such as the higher moments of the entropy or the center of mass of the population, may be better suited in order to extract additional information on the spatial convergence.

A deeper understanding of the spatial behaviour of the neutron population during Monte Carlo power iteration has been achieved by resorting to the theory of branching processes, which allows formally relating the spatial moments (the square pair distance and the square center of mass) to the system parameters. The developed formalism is amenable to exact results (within the diffusion approximation) that are in fairly good agreement with the behaviour observed in the homogeneous cube model.

We have also tested our theoretical findings on more realistic reactor configurations, including a full reactor core and a fuel rod. For the former, we have shown that the formulas derived for a homogeneous cylindrical reactor with reflecting boundaries can capture the scaling of the center of mass fluctuations with respect to the number of particles per generation, although our predictions globally overestimate the fluctuation amplitude. We conjecture that this discrepancy is due to the approximation of having assumed reflecting boundaries: more

sophisticated formulas allowing for arbitrary boundary conditions would be needed, and this issue will be the subject of future research work. Finally, in the case of the fuel rod (with reflective boundaries) our simplified model is actually capable of correctly assessing the amplitude of the center of mass fluctuations and their scaling with respect to the number of simulated particles per generation and to the fuel rod length.

Acknowledgments

E. D., M. N. and A. Z. thank AREVA and Electricité de France (EDF) for partial financial support. J. M., B. F. and K. S. thank the Consortium for Advanced Simulation of Light Water Reactors (CASL), an Energy Innovation Hub for Modeling and Simulation of Nuclear Reactors under U.S. Department of Energy Contract No. DE-AC05-00OR22725, for providing partial financial support.

Appendix A. Expectation of the Shannon Entropy

We develop the calculations for the expected Shannon Entropy \mathcal{S}_N as defined in Eq. (1). Assume that there are B tally regions in the system, with N identical neutrons. The probability for each neutron to be found at region i is P_i . After each simulation, P_i is estimated as

$$\widehat{P}_i = \frac{k_i}{N} \quad (\text{A.1})$$

where k_i is the number of neutrons in region i . Therefore, for the expected entropy we have

$$\begin{aligned} \mathcal{S}_N &= -\mathbb{E} \left[\sum_{i=1}^B \widehat{P}_i \log_2(\widehat{P}_i) \right] \\ &= \log_2(N) - \frac{1}{N} \sum_{i=1}^B \mathbb{E} [k_i \log_2(k_i)]. \end{aligned} \quad (\text{A.2})$$

For each region i , k_i represents the number of occurrences of a neutron fallen in this region. As such, it can be expressed as a sum of N binomial random variables. Therefore, we obtain

$$\mathbb{E} [k_i \log_2(k_i)] = \sum_{k_i=0}^N \binom{N}{k_i} (1 - P_i)^{N-k_i} P_i^{k_i} k_i \log_2(k_i). \quad (\text{A.3})$$

For the homogeneous reactor model considered in Section 2, we simply have $P_i = 1/B$ and \mathcal{S}_N reduces to

$$\mathcal{S}_N = \log_2(N) - \frac{B}{NB^N} \sum_{k_i=0}^N \binom{N}{k_i} (B-1)^{N-k_i} k_i \log_2(k_i). \quad (\text{A.4})$$

Appendix B. The pair correlation function

Let us select a pair of (distinct) neutrons located at positions \mathbf{x} and \mathbf{y} , at time t . These neutrons may, or may not, have had a common ancestor (from a branching event) at a previous time

$0 < t' < t$. Because of the particle number conservation imposed by population control, the fraction of new particle pairs created in the time interval $(t', t' + dt)$ is $\beta dt / (N - 1)$ (Meyer et al., 1996). As a shorthand, we will denote $\beta_p = \beta / (N - 1)$. The probability for a chosen pair of particles at time t not to have had a common ancestor is $e^{-\beta_p t}$, so that the probability density for the ancestor to occur at time t' for a particle pair observed at t is

$$\psi_t(t') = \beta_p e^{-\beta_p(t-t')}. \quad (\text{B.1})$$

The function $h(\mathbf{x}, \mathbf{y}, t)$ can be decomposed as $h = h^{(1)} + h^{(2)}$, where $h^{(1)}(\mathbf{x}, \mathbf{y}, t) = e^{-\beta_p t} h_{id}(\mathbf{x}, \mathbf{y}, t)$ is the contribution of neutrons having evolved freely with no common ancestors. The correlated contribution reads

$$\begin{aligned} h^{(2)}(\mathbf{x}, \mathbf{y}, t) &= N(N-1) \int_0^t dt' \int_V d\mathbf{x}' \mathcal{G}(\mathbf{x}, \mathbf{x}', t-t') \times \\ &\mathcal{G}(\mathbf{y}, \mathbf{x}', t-t') \psi_t(t') \rho(\mathbf{x}', t'). \end{aligned} \quad (\text{B.2})$$

where $N(N-1)\psi_t(t')dt'$ is the number of ordered particle pairs at time t that have a common ancestor in the time interval $(t', t' + dt')$. The pair correlation function finally yields

$$h(\mathbf{x}, \mathbf{y}, t) = \frac{N(N-1)}{V^2} e^{-\beta_p t} + \beta \frac{N}{V} \int_0^t dt' e^{-\beta_p t'} \mathcal{G}(\mathbf{x}, \mathbf{y}, 2t')$$

when imposing $Q = 1/V$.

References

- Athreya, K.B., Ney, P., 1972. Branching processes. Grundlehren Series, Springer-Verlag, New York.
- Bell, G.I., Glasstone, S., 1970. Nuclear reactor theory, Van Nostrand Reinhold Company, New York.
- Brown, F., 2005. LA-UR-05-4983, Los Alamos National Laboratory.
- Brown, F., 2009. Proceedings of M&C2009, Saratoga Springs, N.Y. USA.
- Brun, E., et al., 2015. Ann. Nucl. Energy **82**, 151-160.
- Chadwick, M.B., (2006). Nuc. Data Sheets **107**, 2931-3060.
- Cover, T.M., Thomas, J.A., 1991. *Elements of information theory*, John Wiley & Sons, New York.
- Dumonteil, E., Courau, T., 2010. Nuclear Technology **172**, 120.
- Dumonteil, E., Malvagi, F., 2012. Proceedings of ICAP2012, Chicago.
- Dumonteil, E., Le Peillet, A., Lee, Y.K., Petit, O., Jouanne, C., Mazzolo, A., 2006. Proceedings of PHYSOR2006, Vancouver.
- Dumonteil, E., Malvagi, F., Zoia, A., Mazzolo, A., Artusio, D., Dieudonné, C., de Mulatier, C., 2014. Ann. Nuc. Energy **63**, 612-618.
- Gelbard E.M., Prael, R., 1990. Prog. Nucl. Energy **24**, 237.
- Grebenkov, D. S., Nguyen, B. T., 2013. SIAM Review **55** 601-667.
- Hoogenboom, J.E., Martin, W.R., 2010. In Proceedings of the International Conference on Mathematics, Computational Methods and Reactor Physics (M&C2009), Saratoga Springs, USA; and Hoogenboom, J.E., Martin, W.R., Petrovic, B., (2010). Benchmark specifications, Revision 1.2.
- Houchmandzadeh, B., 2008. Phys. Rev. Lett. **101**, 078103.
- Jacquet, O., Chajari, R., Bay, X., Nourri, A., Carraro, L., 2000. Proceedings of ICRS2000, Lisbon.
- L'Abbate, A., Courau, T., Dumonteil, E., 2007. Proceedings of PHYTRA1, Marrakech.
- Li and Vitanyi, 1997. An Introduction to Kolmogorov Complexity and Its Applications, Springer.
- Lux, I., Koblinger, L., 1991. Monte Carlo particle transport methods: Neutron and photon calculations, CRC Press, Boca Raton.
- Miao, J., Forget, B. and Smith, K., 2016. Ann. Nuc. Energy **92**, 81-95.
- Meyer, M., Havlin, S., Bunde, A., 1996. Phys. Rev. E **54**, 5567.
- de Mulatier, C., Dumonteil, E., Rosso, A., Zoia, A., 2015. J. Stat. Mech. P08021.

- Pázsit, I., Pál, L., 2008. Neutron Fluctuations: A Treatise on the Physics of Branching Processes, Elsevier, Oxford.
- Rief, H., Kschwendt, H., 1967. *Nuc. Sci. Eng.* **30**, 395-418.
- 645 Shi, B., Petrovic, B., 2010. In Proceedings of the ANS International Conference on the Physics of Reactors (PHYSOR 2010), Pittsburgh, PA, May 9-14 (2010).
- Shi, B., Petrovic, B., 2010. In Proceedings of the Joint International Conference on Supercomputing in Nuclear Applications and Monte Carlo 2010 (SNA+MC2010), Tokyo, Japan, October 17-21, 2010.
- 650 Sjenitzer, B.L., Hoogenboom, J.E., 2011. *Ann. Nucl. Eng.* **38**, 2195.
- T. M. Sutton, 2014. In Proceedings of the SNA+MC2013 conference, Paris, France.
- TRIPOLI-4 Project Team, 2008. TRIPOLI-4 User guide, Rapport CEA-R-6169.
- Ueki, T., Brown, F., 2003. Proceedings of M&C2003, Gatlinburg, Tennessee.
- 655 Ueki, T., Brown, F., Parsons, D.K., Kornreich, D.E., 2003. *Nucl. Sci. Eng.* **145**, 279.
- Ueki, T., Brown, F., Parsons, D.K., Warsa, J.S., 2004. *Nucl. Sci. Eng.* **148**, 374.
- Ueki, T., 2005. *Nucl. Sci. Eng.* **151**, 283.
- Ueki, T., 2012. *J. Nucl. Sci. Tech.* **49**, 1134-1143.
- 660 Wenner, M., Haghghat, A., 2007. *Trans. Am. Nuc. Soc.* **97**, 647-650.
- Wenner, M., Haghghat, A., 2008. In Proceedings of the Physor2008 conference, Interlaken Switzerland.
- Williams, M.M.R., 1974. *Random Processes in Nuclear Reactors*, Pergamon Press, Oxford.
- 665 Young, W.R., Roberts, A.J., Stuhne, G., 2001. *Nature*, **412**, 328.
- Zhang, Yi-C., Serva, M., Polikarpov, M., 1990. *J. Stat. Phys.* **58**, 849-861.
- Zoia, A., Dumonteil, E., Mazzolo, A., Mohamed, S., 2012. *J. Phys. A: Math. Theor.* **45**, 425002.
- 670 Zoia, A., Dumonteil, E., Mazzolo, A., de Mulatier, C., Rosso, A., 2014. *Phys. Rev. E* **90**, 042118.